Published by Avanti Publishers

Journal of Advanced Thermal Science Research

ISSN (online): 2409-5826

Research on the Characteristics of Fire Detection and Alarm Devices Based on the Thermoacoustic Effect

Xueqiang Shi[1,*], Xuhui Ren[2], Biao Shi[1], Bin Chi[3], Kaishu Huang[4], Wenhai Li[5], Yutao Zhang[2,*], Yali Li[1], Mucong Deng[6], Weiguo Cao[1] and Hongzhen Duan[7,*]

[1]School of Environment and Safety Engineering, North University of China, Taiyuan 030051, Shanxi, China; [2]School of Safety Science and Engineering, Xi'an University of Science and Technology, Xi'an 710054, Shaanxi, China; [3]China International Engineering Consulting Corporation, Beijing 100048, China; [4]Chongqing Hongyu Precision Industry Co. Ltd, Chongqing 402760, China; [5]China Safety Technology Research Academy of Ordnance Industry, Beijing 100053, China; [6]College of Shipbuilding Engineering , Harbin Engineering University, Harbin 150001, China; [7]School of Chemistry & Chemical Engineering, North University of China, Taiyuan 030051, Shanxi, China

ARTICLE INFO

Article Type: Research Article

Academic Editor: Huan Xi

Keywords:
Heat transfer
Sound pressure
Numerical simulation
Thermoacoustic effect
Fire detection and alarm

Timeline:
Received: September 09, 2025
Accepted: November 19, 2025
Published: November 28, 2025

Citation: Shi X, Ren X, Shi B, Chi B, Huang K, Li W, Zhang Y, Li Y, Deng M, Cao W, Duan H. Research on the characteristics of fire detection and alarm devices based on the thermoacoustic effect. J Adv Therm Sci Res. 2025; 12: 53-72.

DOI: https://doi.org/10.15377/2409-5826.2025.12.4

ABSTRACT

The thermoacoustic effect can convert heat in a fire into sound energy, which has considerable application prospects in fire detection. A fire detection and alarm device based on thermoacoustic effect has been developed for building fire prevention. The main content of thermoacoustic effect is briefly introduced, and the application of thermoacoustic devices in fire detection is explained. A fire detection and alarm device based on thermoacoustic effect has been established. The total length of the entire device is 330 mm, with a uniform inner diameter of 40 mm. Finite element numerical simulation software is used to calculate and analyze detection and alarm devices. The characteristics of sound pressure level changing with the temperature difference of the heat exchanger were analyzed, and then the experimental, theoretical, and simulated sound response frequency values were calculated. Numerical simulations demonstrate the nonlinear multi field coupling characteristics in the process of thermoacoustic conversion. The established device begins to produce sound under the condition of a temperature difference of 194 ℃ in the heat exchanger, with a sound pressure level of 120 dB. Numerical simulation can better reflect the sound pressure level and frequency characteristics of the device. The distribution characteristics of flow and temperature can effectively demonstrate nonlinear dissipation properties. Thermoacoustic conversion exhibits characteristics of compression and heat transfer at a small scale. Thermoacoustic devices can convert the heat in a fire into acoustic alarm signals, and have great potential for application in the field of fire alarm in the future. This study provides new ideas for the construction of new fire alarm devices and important theoretical basis for the research of thermoacoustic alarm devices.

*Corresponding Authors
Email: shixueqiang@nuc.edu.cn (Xueqiang Shi); ytzhang@xust.edu.cn (Yutao Zhang); duanhz2000@163.com (Hongzhen Duan)
Tel: +(86) 19303433552

1. Introduction

With the development of cities and the use of various flammable materials, the casualties caused by fire accidents are more than 20 times the total number of natural disasters such as floods and earthquakes, making it the main accident disaster facing humanity today [1, 2]. To effectively and timely detect and alarm fires, various fire detection and alarm systems are applied, such as smoke detectors, temperature detectors, visual detectors, etc [3]. The above-mentioned fire detectors themselves are relatively complex instruments that require power connection, and the detection and alarm of fires require several modules to be interconnected, which undoubtedly increases the complexity and instability of the system. Some devices are also susceptible to environmental influences and can only be used in specific environments [4]. Compared with conventional detection and alarm devices, the fire detection and alarm device based on thermoacoustic conversion has no moving parts, simple structure, no mechanical losses such as friction, improves the service life of the device, does not require power supply, and reduces energy consumption. The thermoacoustic device directly utilizes the heat generated by combustion, thus ensuring a certain degree of accuracy and accurately detecting fire accidents [5, 6]. Thermoacoustic devices rely on thermoacoustic effects, namely the interaction between oscillating working fluids and unevenly heated porous materials, to induce high-intensity self-excited acoustic oscillations, which can be further used for power generation [7, 8], heat transfer [9], refrigeration [10, 11], etc. Thermoacoustic devices can be mainly divided into two categories based on their core structure: standing wave type thermoacoustic devices and traveling wave type thermoacoustic devices [12, 13]. The main difference between these two structures is that the propagation mode of sound waves (pressure waves) inside the device is different from the coupling mode of thermal cycles, resulting in significant differences in performance and efficiency [14, 15]. The structure of the standing wave thermoacoustic device is relatively simple and suitable as an alarm device for fires.

Traditional fire alarm technology has some problems, and thermoacoustic devices can compensate for the shortcomings of existing alarm devices and have potential application value in fire alarm. It is meaningful to conduct research on fire alarm devices based on thermoacoustic effects. The concept of thermoacoustics and the structural composition of thermoacoustic engines were introduced, and the application of standing wave thermoacoustic engines in fire detection and alarm was commented upon. In order to further study the thermoacoustic detection and alarm device in experiments and theory, a thermoacoustic device was designed and validated using numerical simulations. The sound pressure level and frequency variation laws were studied, and the multi field coupling characteristics of the device were discussed. This research can provide new solutions to make up for many problems of traditional alarm devices and offer an important theoretical basis for the study of thermal acoustic alarm devices.

1.1. Thermoacoustic Effect

Thermoacoustics mainly studies the mutual conversion between heat and sound to improve energy utilization and system cooling [16]. Thermoacoustic conversion is a time averaged energy conversion, which means that when the appropriate phase angle is met for heat input and gas motion, compressible fluids can produce acoustic oscillations through thermal interactions with solid media [17, 18]. Rott proposed a linear thermoacoustic theory based on temperature gradient and transverse thermal penetration depth that is shorter than the wavelength of the acoustic wave, which can explain the working conditions of most thermoacoustic engines [19]. Swift proposed the concept of critical temperature, which supplements the classical linear thermoacoustic theory. The critical temperature is expressed as [5, 16]:

$$\nabla T_{crit} = \frac{T_m \alpha_p w p_1^s}{\rho_m C_p u_1^s} \tag{1}$$

where, T_m is the average temperature, α_p is the coefficient of thermal expansion, w is the oscillation angular frequency, ρ_m is the density, C_p indicates the specific heat capacity at constant pressure of the gas, p_1^s and u_1^s are the pressure and velocity amplitudes, respectively.

According to the conversion relationship between heat and sound, thermoacoustic devices can be divided into thermoacoustic engines and thermoacoustic refrigerators. Thermoacoustic engines output sound power (W) and

waste heat (Q_0) at lower temperatures under the condition of a heat source (Q_h) input, while thermoacoustic refrigerators operate on the opposite principle, relying on pressure to extract excess heat from the system (Eq. 2).

$$Q_h \rightarrow Q_0 + W \tag{2}$$

At the mesoscale, a simplified analysis of thermoacoustic conversion is carried out by active small air masses in the plate stack. Fig. (**1**) shows the operation process of a standing wave thermoacoustic engine. The plate stack can be simplified as two flat plates (Fig. **1a**, **1b**). Assuming that when the temperature difference (∇T_d) between the plates is greater than the critical temperature (∇T_{crit}), the system is in steady-state vibration and there is a pressure change during the cycling process. Throughout the entire process in a-b-c-d order, active small air masses expand or contract under the influence of temperature differences and velocity waves, resulting in pressure fluctuations. In this Brayton cycle, gas clusters absorb heat at high temperatures and release heat and do work at low temperatures. When countless gas clusters move, the device generates acoustic work (Fig. **1c**, **1d**).

To study the thermoacoustic effect more effectively and optimize the thermoacoustic device, a series of simulation studies were conducted on the thermoacoustic device [20, 21]. DeltaEC is an important software for optimizing thermoacoustic devices, mainly using one-dimensional acoustic approximation to numerically integrate the wave equation and energy equation, which can calculate the efficiency of complex thermoacoustic devices [22]. Due to the complexity of the thermoacoustic effect and the nonlinear characteristics it induces, numerical simulation methods have been widely applied [23]. Guo *et al*. used CFD technology to construct two-dimensional and three-dimensional time-domain models and conducted numerical simulations on Stirling traveling wave and standing wave thermoacoustic engines, exploring the mode transitions caused by mass flow and external flow disturbances [24]. Baltean-Carlès *et al*. used numerical simulation methods to study the influence of gravity on thermoacoustic devices, and analyzed the performance effects of temperature and flow fields on thermoacoustic energy conversion under different directions of gravity [25]. Blanc *et al*. conducted a two-dimensional simulation of a high amplitude standing wave thermoacoustic engine using PyFR, exploring nonlinear effects such as Rayleigh flow, jet flow, and high-order harmonics [26].

So far, thermoacoustic theory has been relatively mature, and thermoacoustic devices have been widely used in microelectronic heat dissipation [27], solar generators [28], and refrigeration air conditioning [29]. Existing relevant theories can guide the construction of thermoacoustic conversion detection alarms and optimize the materials and geometric parameters of their components.

The current research on thermoacoustic effects and devices mainly focuses on experiments and numerical simulations. However, there is not much research on the design, construction, and testing of the structure of thermoacoustic alarm devices. In addition, there is less research on numerical simulation of thermoacoustic alarm devices in fire scenarios.

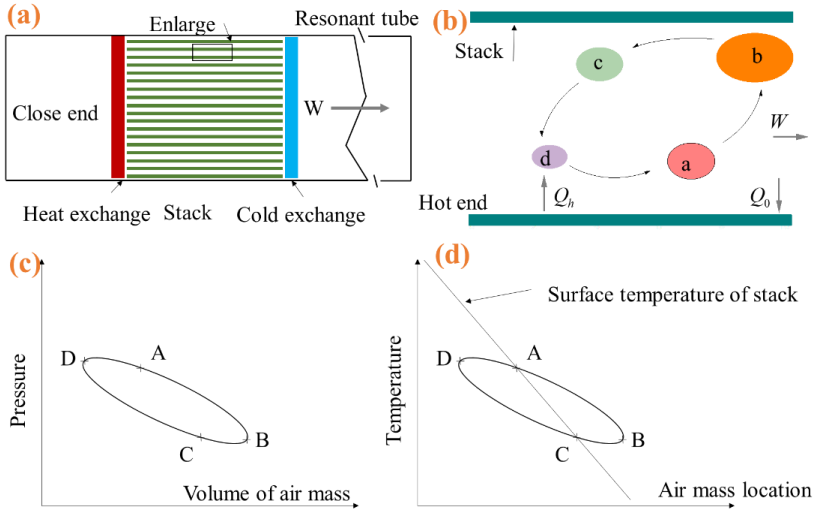

Figure 1: Operation process of standing wave thermoacoustic engine.

1.2. Application of Standing Wave Thermoacoustic Engine in Fire Detection and Alarm

When a building fire occurs, the smoke generated by combustion accumulates in the upper part, forming a high-temperature smoke layer. Such high temperature can trigger the thermoacoustic device to emit an alarm sound signal, achieving passive alarming. Existing research has applied thermoacoustic engines to fire detection and alarm systems. Buda-Ortins from the University of Maryland developed a model of a firefighter's head-mounted flashover detector based on thermoacoustic conversion [30]. The temperature and acoustic characteristics of the thermoacoustic engine were analyzed under heat source input powers of 44 W and 31 W, respectively. The sound level measured during the test was 115 dB at 500 Hz. Hamburger optimized the device developed by Buda-Ortins [31]. To simplify the device, they removed the cold-end heat exchanger during the experiment and reset the geometric parameters. In the experiment, it was found that the addition of water would make the thermoacoustic device easier to emit sound. Additionally, the heat pipe and heat collector were added, and their efficiency was theoretically analyzed. Jeffrey tested the impact of different stack filling materials on the temperature difference during sound generation [32]. To test the actual effectiveness of the heat pipe and heat collector, the entire prototype of the thermoacoustic flaming detector was tested sequentially in a radiant panel and then in an actual fire room. Unfortunately, these related studies did not determine the optimal materials and parameters for the thermoacoustic engine, but only proposed the initial prototype. The previous work involved the design of thermoacoustic alarm devices, analysis of thermoacoustic effect theory, and so on. However, there are still shortcomings in the acoustic characteristics and related theoretical research on the response of thermoacoustic devices in fire scenarios. Furthermore, there is a lack of numerical theoretical analysis on the thermoacoustic effects of thermoacoustic devices in fire scenarios.

In the context of fire, more scientific evidence is needed to support the application of thermoacoustic engines in fire scenes. 1) How to more effectively collect heat from the fire scene and transfer it to the thermoacoustic detection alarm; 2) Design a thermoacoustic detection alarm with the most reasonable geometric configuration at the initial temperature of fire spread; 3) Optimize the thermoacoustic engine by removing redundant components to simplify its structure; 4) The sound propagation characteristics need to be considered [33]. How should the heat sound detection alarm be set up in the room so that it can transmit the loudest sound to the personnel. 5) After adding water, the temperature difference between the hot end and the cold end of the thermoacoustic engine, which is capable of producing sound, will be greatly reduced [34, 35]. Currently, the temperature difference can reach a minimum of around 90 ℃, and water can be used to guide the entire device to start oscillating. This work carefully compared the research results of predecessors and intends to supplement and solve the following problems: (1) The design of thermoacoustic alarm devices for fire scenarios. (2) Acoustic response characteristics of the designed thermoacoustic alarm device. (3) Numerical simulation of thermoacoustic alarm device to supplement detailed heat transfer, flow, and acoustic information.

By summarizing the basic theory of thermoacoustic conversion, analyzing the development of thermoacoustic engines in fire detection and alarm, a fire detection and alarm device based on the thermoacoustic effect was built, and experiments and numerical simulations of the thermoacoustic device were carried out. The research results are of great significance for guiding the optimization and application of fire detection and alarm devices based on the thermoacoustic effect.

2. Experimental Instruments and Numerical Methods

2.1. Design Principles of Standing Wave Thermoacoustic Engines

Since fire detection alarms only need to convert heat into sound, in order to simplify the structure and meet the requirements of fire detection and alarming, a quarter-wavelength standing wave thermoacoustic engine has been developed. A thermoacoustic engine primarily consists of four components: a sealed gas chamber (Hot buffer), a stack frame, a porous medium stack, and a resonance tube [36]. In practical applications, both ends of the stack are also equipped with hot-end heat exchangers and cold-end heat exchangers. The stack is the core component of the entire thermoacoustic engine, and its function is to create a temperature gradient within the device [37]. It is the primary location where time-averaged heat flow and time-averaged acoustic flow are

transformed. The hot-end heat exchanger transfers heat from the external fire field to the thermoacoustic engine, forming the high-temperature end of the stack. The cold-end heat exchanger extracts the excess heat from the stack, forming the low-temperature end of the stack [38]. The resonator amplifies the pressure wave generated by the stack and modulates it into acoustic power consistent with the geometric parameters of the resonator.

The design basis of the thermoacoustic fire detection and alarm device mainly includes the following contents.

1) Tightness: Jung *et al*. designed a small prototype of a thermoacoustic engine. In his design, the entire device requires good tightness, meaning that there must be no airflow leakage at the closed end, otherwise the device will not be able to generate sound [39];
2) Stack material: The thermal capacity of the stack should be high enough to accommodate heat movement across the stack, but its thermal conductivity should be low enough to reduce heat conduction between the stacks, thereby reducing power consumption. Common stack materials include metals and ceramics, etc. [40];
3) Stack spacing: The thermoacoustic effect occurs within a range of one thermal penetration depth from the stack. When the spacing between stacks is too large, it can have a certain impact on the thermal conversion efficiency. Generally, a spacing of 2 to 4 times the thermal penetration spacing is optimal [41];

$$\delta_k = \sqrt{\frac{2\alpha}{w}} = \sqrt{\frac{k}{\pi f \rho C_p}} \tag{3}$$

where, α represents the thermal diffusivity, w denotes the oscillation angular frequency, and $w = 2\pi f$. k signifies the thermal conductivity of the gas, ρ stands for the density of the gas, C_p indicates the specific heat capacity at constant pressure of the gas, f is the acoustic vibration frequency, and δ_k typically takes a value of a few tenths of a millimeter.

4) Center position of stack: The center of the stack should be located at the pressure antinode of the standing wave, with a typical value between x = 0 m and x = λ / 8 m (λ is the wavelength of sound) [42];
5) Smoothness: When the interior of a thermoacoustic engine is not smooth, it increases viscous dissipation and may induce unstable flow, thereby affecting the temperature field distribution. Therefore, the interior of the thermoacoustic engine should be made as smooth as possible.
6) Resonator: The material of the resonator should be hard and non-absorbent to sound, and the length of the resonator should be 1/4 of the wavelength of sound.

2.2. Experimental Setup

The thermoacoustic detection alarm is a quarter-wavelength thermoacoustic engine, and also a type of mechanism with no moving parts [43]. Fig. (**2a**) is a physical image of the thermoacoustic alarm device used in the experiment, and Fig. (**2b**) is a schematic diagram of the thermoacoustic alarm device used in the experiment. The stack is the primary site for thermoacoustic energy conversion. Table **1** presents the parameters of various components in the standing wave thermoacoustic engine. The stack is formed by winding stainless steel wire. The temperature difference across the stack induces incomplete heat transfer between the gas within the stack and the stack itself, thereby triggering thermoacoustic oscillations [44, 45]. In the experiment, the hot-end heat exchanger was heated using a heating rod, while the cold-end heat exchanger employed a water-cooling structure. The total length of the entire device is 330 mm, with a uniform inner diameter of 40 mm.

Use K-type patch thermocouples (GG-K-36-SLE, error: 1.1℃ or 4%) to measure the temperature of the heat exchangers at both ends of the plate stack (hot-end heat exchanger and cold-end heat exchanger), and employ an AWA6228+ multifunction sound level meter (AWA6228+, error: 1.2%) to determine the acoustic characteristics. The experiment was conducted in a stable and quiet environment, using a power source to supply power to the heating rod to increase its temperature and simulate a fire scene. The cold end of the thermoacoustic device is equipped with a water cooling device to ensure a lower temperature, resulting in a considerable temperature

difference between the hot and cold ends. In the experiment, thermocouples were used to test the temperature of the hot and cold ends, and a sound level meter was used to test the acoustic information. The testing locations for temperature and acoustic parameters are shown in Fig. (**2b**). Interestingly, when the temperature difference between the hot and cold ends reaches a certain value, the thermoacoustic device emits an alarm sound. By changing the temperature difference between the hot and cold ends in each experiment, acoustic information can be obtained under different temperature difference conditions.

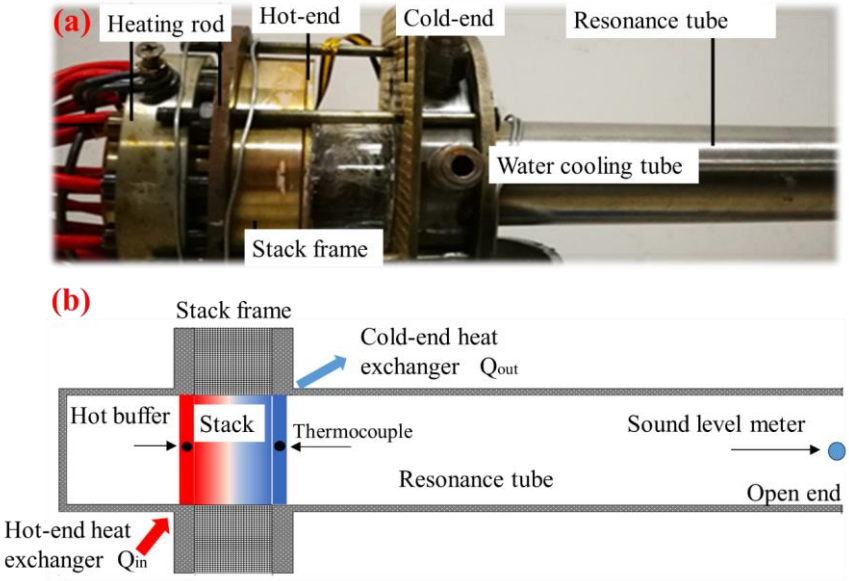

Figure 2: The physical and schematic diagram of the thermoacoustic alarm device used in the experiment.

Table 1: Parameter of components in design standing wave thermoacoustic engine.

Component	Material	Length (mm)	Outer Diameter (mm)
Heating rod	Stainless steel	45	10
Hot-end heat exchanger	Copper	12	90
Gas chamber	Copper	60	50
Stack frame	High-temperature resistant quartz glass	26	50
Cold-end heat exchanger	Copper	12	110
Resonance tube	Stainless steel	235	42
Water cooling device	Stainless steel	20	90

2.3. Numerical Simulation

To investigate the multi-physics characteristics of the thermoacoustic response of the thermoacoustic detection and alarm device in detail, a 2D transient low Mach number compressible flow quarter-wavelength model was established using COMSOL Multiphysics. The adopted flow model is Implicit Large Eddy Simulation (ILES), with the turbulence properties for heat transfer set to Kays-Crawford, and solved using the PARDISO solver [46, 47].

The interior of a thermoacoustic engine mainly involves the coupling of heat transfer and flow, which is solved by combining the continuity equation, momentum equation, and energy equation. The pressure, velocity, and density in the model vary with the response of the system, and the Navier Stokes equations are used to control the fluid flow conditions:

$$\frac{\partial \rho}{\partial t} + \nabla(\rho \mathbf{u}) = 0 \tag{4}$$

$$\rho \frac{\partial \mathbf{u}}{\partial t} + \rho(\mathbf{u} \cdot \nabla)\mathbf{u} = \nabla \cdot [-p\mathbf{I} + \mu(\nabla \mathbf{u} + (\nabla \mathbf{u})^T) - \frac{2}{3}\mu(\nabla \mathbf{u})\mathbf{I}] + \mathbf{F} \tag{5}$$

The energy equation is expressed as:

$$\rho C_p \frac{\partial T}{\partial T} + \rho C_p \mathbf{u} \cdot \nabla T - \nabla(k \nabla T) = Q + q_0 Q_p + Q_{vh} \tag{6}$$

where, ρ is the gas density, μ is the aerodynamic viscosity, p is the pressure, T is the temperature, C_p is the constant pressure heat capacity, k is the thermal conductivity, Q_{vh} is the viscous dissipation heat generation term, Q_p is the pressure work heat generation term, and Q is the heat source. The bold font indicates that the parameter is a vector. **u** represents the velocity field. **F** represents volumetric force. **q** represents the heat flux vector. **I** is a unit matrix.

The calculation method for additional energy in the equation is expressed as:

$$Q_p = \alpha_p T(\frac{\partial p}{\partial t} + \vec{u} \cdot \nabla p) \tag{7}$$

$$\alpha_p = -\frac{1}{\rho}(\frac{\partial \rho}{\partial T})_p \tag{8}$$

$$Q_{vd} = \tau : \nabla \vec{u} \tag{9}$$

where, τ and α_p are the viscous tensor and the thermal expansion coefficient, respectively. Table **2** shows the boundary conditions for numerical simulation. f_0 is normal stress. ΔH is the sensible enthalpy.

Table 2: Boundary conditions for numerical simulation.

Boundary Conditions	Fluid Heat Transfer	Fluid Flow
Wall surface (hot buffer/ resonance tube)	$-\boldsymbol{n} \cdot \boldsymbol{q} = 0$	$\boldsymbol{u} = 0$
Stack surface	$T = T_0$	$\boldsymbol{u} = 0$
Open boundary	$-\boldsymbol{n} \cdot \boldsymbol{u} < 0; -\boldsymbol{n} \cdot \boldsymbol{q} = \rho \Delta H \boldsymbol{u} \cdot \boldsymbol{n}$ $-\boldsymbol{n} \cdot \boldsymbol{u} \geq 0; -\boldsymbol{n} \cdot \boldsymbol{q} = 0$ $\Delta H = \int_{T_{ustr}}^{T} C_p dT$	$[-p\boldsymbol{I} + \boldsymbol{K}]\boldsymbol{n} = -f_0 \boldsymbol{n}$

Fig. (**3**) shows the numerical model and its element results, with the model comprising 19,152 domain elements. To simplify the calculation, the stack is assumed to consist of 19 plate-like structures, which is also a commonly used method for simplification [48, 49]. The other geometric structures were the same as those used in the experiment. To enable the system to self-excite at the beginning and reduce the computational load of the model, an initial linear temperature gradient is set at both ends of the plate stack. In order to simplify numerical simulation and eliminate unnecessary computational costs, the model only considers the hot buffer, plate stack, and resonance tube, which is also a commonly used simulation strategy for thermoacoustic heat engines [50]. The elements of the model are shown in Fig. (**3**), with structured elements set at the plate stack and unstructured elements in other areas. The elements were analyzed using skewness, with colors representing skewness values. In the subsequent work, select point A and its horizontal and vertical intercepts for detailed analysis.

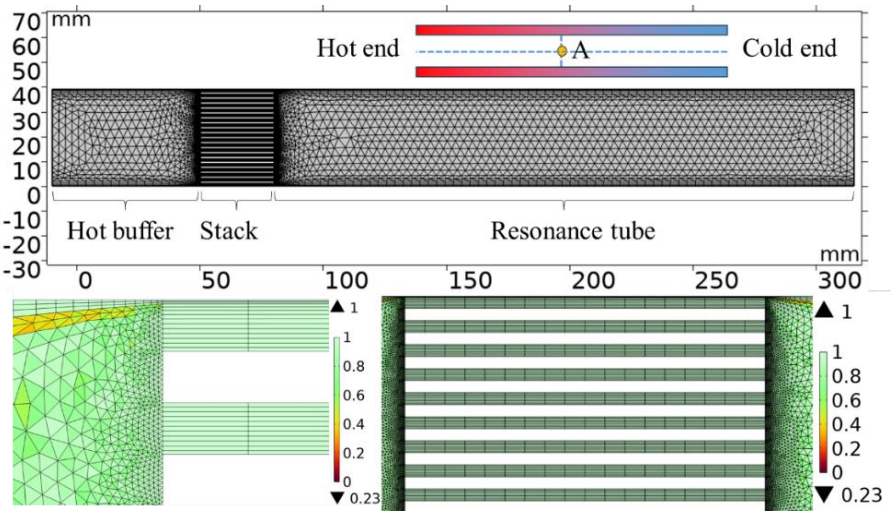

Figure 3: The numerical model and its element results.

3. Results and Discussion

3.1. Acoustic Characteristics of Experimental Results

The sound pressure level of the alarm device determines the effectiveness of the alarm. Fig. (**4**) shows the variation of sound pressure level of the thermoacoustic flaming detection alarm device under different temperature differences (Δ*T*) of the heat exchangers at both ends of the plate stack. The change in sound pressure level is divided into three stages: Energy storage, rapid rise, and saturation. During the energy storage stage, the device did not produce any sound because under this temperature difference condition, the plate stack and gas heat and mass transfer did not cause strong pressure oscillations. The conversion of thermal and kinetic energy in the stack did not overcome the impedance of the system. The temperature difference of the heat exchanger that can produce sound is about 194℃, and its sound pressure level is about 121 dB. As the temperature difference increases, the sound pressure level shows an increasing characteristic, known as the rapid rise stage. The temperature difference range during the rapid rise stage is 194 ~ 231 ℃. The conversion between thermal energy and kinetic energy overcomes system impedance, and as thermal energy increases, kinetic energy also increases. In the saturation stage, even if the temperature difference further increases, the sound pressure level

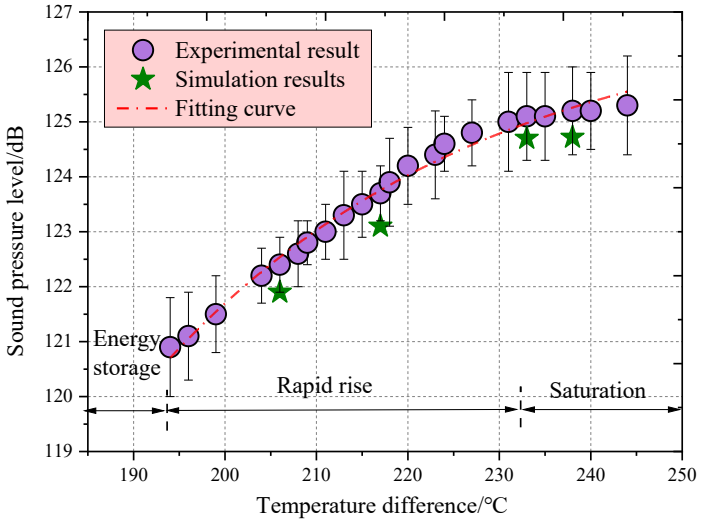

Figure 4: The variation of sound pressure level of the thermoacoustic flaming detection alarm device under different temperature differences.

does not change much. This indicates that under the configuration of the system, energy conversion has reached saturation. When the temperature difference is greater than 231℃, the sound pressure level remains stable around 125.1 dB. Compared with experimental values, although there are some errors in the simulation, it can better qualitatively and quantitatively represent the variation pattern of sound pressure level. Fit the sound pressure level (*SPL*) results and temperature difference (∇T_d) to obtain a fitting formula with a goodness of fit R^2 of 0.98866.

$$SPL = -1454.6\, exp(-\frac{\nabla T_d}{35.8}) + 127.14 \tag{10}$$

By performing fast Fourier transform (FFT) on the measured acoustic signal, the frequency characteristics of the thermoacoustic detection alarm device are obtained. Fig. (**5**) shows the response frequency of the constructed device. The main frequency of the acoustic response of the thermoacoustic detection alarm device is 281.3 Hz, and in addition, there are four secondary frequencies in the high frequency range. Eq. (5) is commonly used in thermoacoustics to calculate the response frequency of thermoacoustic devices [35].

$$f = \frac{a}{4L} = \frac{\sqrt{kRT}}{4L} \tag{11}$$

where, *a* is the speed of sound, m/s, *L* is the length of the total thermoacoustic device, the length of the thermoacoustic device in this work is 330 mm, *k* is the thermal conductivity of the gas, W/(m· K), *R* is the gas constant, J/(mol· K), *T* is the gas temperature, K. The response frequency *f* calculated by Eq. (5) is 261.5 Hz. It is worth mentioning that the acoustic frequency calculated in the numerical simulation is 273.06 Hz. Obviously, the numerical simulation results are more similar to the experimental results.

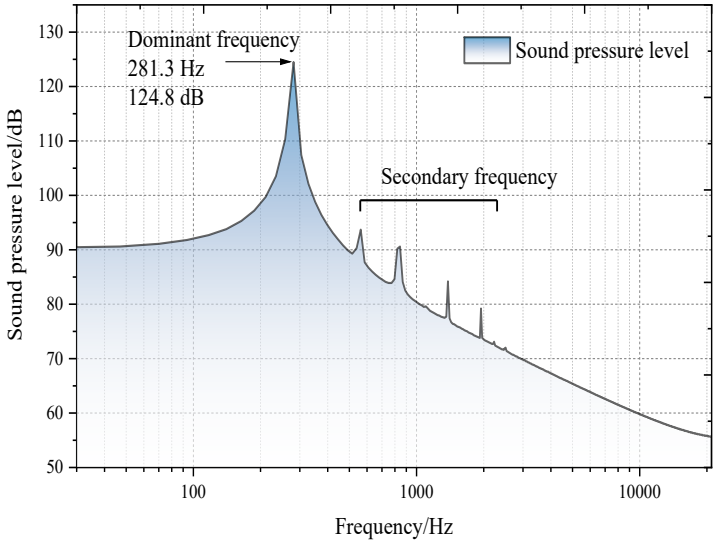

Figure 5: The response frequency of the constructed device in the experiment.

3.2. Energy Characteristics of Thermoacoustic Conversion

In the thermoacoustic conversion process of a thermoacoustic engine, thermal energy is converted into kinetic energy. The manifestation of kinetic energy is periodic pressure waves, also known as sound waves. Fig. (**6**) shows the pressure variation characteristics at point A in the center of the laminated channel. Due to the unstable heat transfer between the plate stack and the fluid in the initial state, the pressure changes are not stable enough, which is called the vibration initiation stage. As the heat transfer between the fluid and the plate stack tends to stabilize, the fluid vibration characteristics also become stable, and the acoustic characteristics exhibit a steady state. In fact, the peak pressure is determined by the heat transfer characteristics at the plate stack, while the acoustic frequency is determined by the resonant tube. Due to the strong heat transfer at the stack, the thermoacoustic conversion is most pronounced here, resulting in a higher pressure at that location.

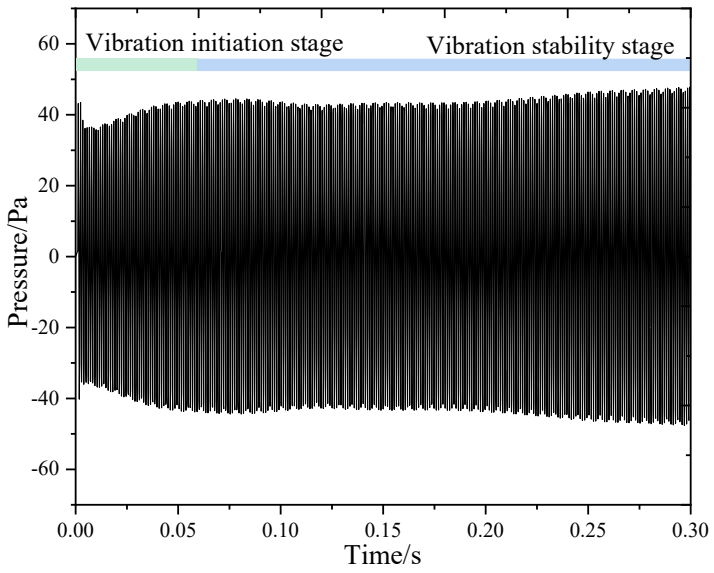

Figure 6: The pressure variation characteristics at point A in the center of the stack channel.

The acoustic frequency is obtained by performing a fast Fourier transform on the pressure characteristics in Fig. (**6**). Fig. (**7**) shows the acoustic frequency of the thermoacoustic device. Due to the simplification of the actual device by the numerical simulation model, there are certain differences between the acoustic frequency distribution characteristics and experimental results. The acoustic main frequency of the experiment is 281.3 Hz, and the acoustic main frequency obtained from numerical simulation is 273.06 Hz. The difference between the acoustic main frequency obtained from numerical simulation and the experimental results is relatively small. The acoustic frequencies obtained from numerical simulations did not exhibit strong sub frequencies.

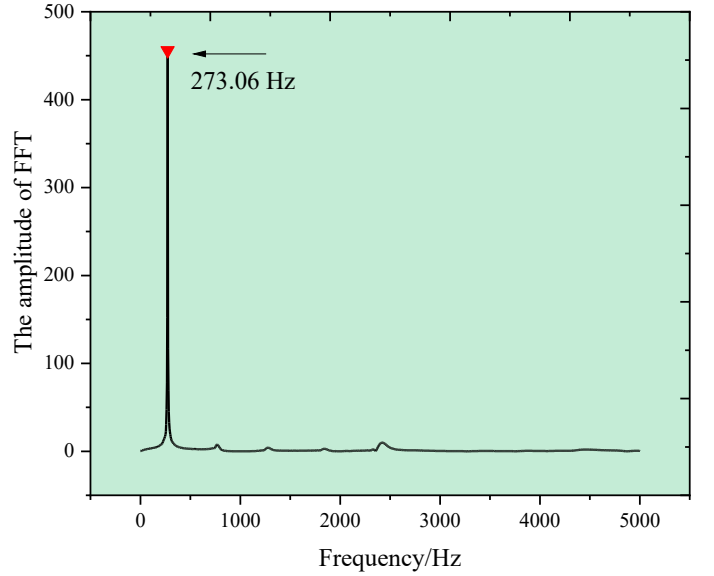

Figure 7: The acoustic frequency of the thermoacoustic device.

In order to demonstrate the energy characteristics during the thermoacoustic conversion process in detail, it is necessary to analyze the multi parameter changes within the acoustic cycle. Fig. (**8**) shows the changes in pressure and key moments during an acoustic cycle. Eight moments (Expressed as Ψ1, Ψ2, Ψ3, Ψ4, Ψ5, Ψ6, Ψ7, Ψ8) were selected within one acoustic cycle to analyze the key parameters within the cycle. Obviously, the variation of acoustic pressure follows a sinusoidal characteristic.

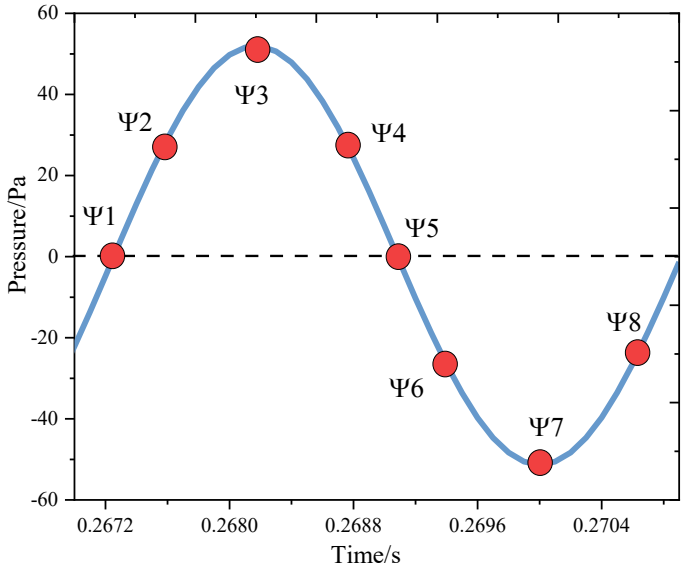

Figure 8: The changes in pressure and key moments during an acoustic cycle.

Plate stacking is the core area of thermoacoustic conversion in thermoacoustic engines. During each acoustic cycle, heat and mass transfer occur between the fluid and the plate stack. Fig. (**9**) shows the temperature variation of the fluid at the cross-section of the plate stack. The horizontal axis represents the height of the stack channel (Vertical intercept line passing through point A, shown in the Fig. **3**), and the vertical axis represents the dimensionless temperature, which is calculated from the temperature of the fluid (T_f) and the stack temperature at that location (T_s). Within an acoustic cycle, the temperature changes of the fluid exhibit periodic characteristics. Acoustic driven fluid undergoes periodic motion in the stack channel, which means that the fluid constantly exchanges heat with the stack at any time. Due to the characteristics of the boundary layer, the fluid temperature at the center of the plate stack channel always lags behind the plate stack temperature. This lagging behavior is determined by the direction of flow. The positive or negative sign of dimensionless temperature represents the direction of heat transfer between the fluid and the plate stack.

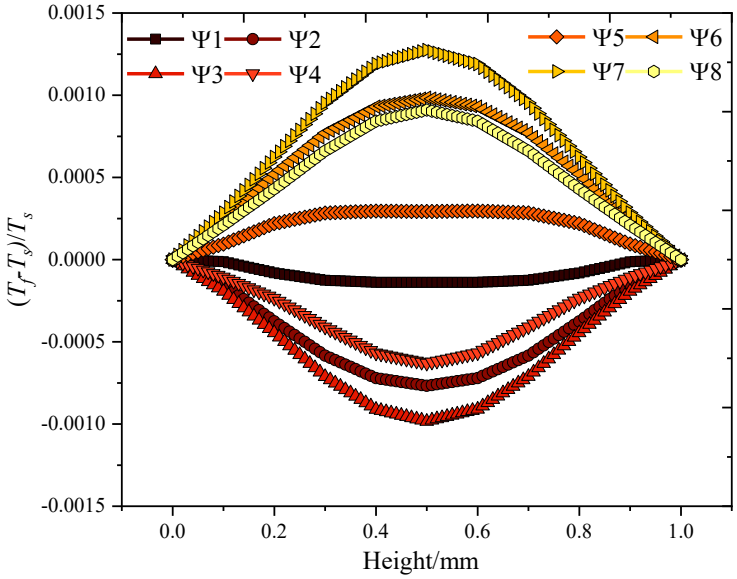

Figure 9: The temperature variation of the fluid at the cross-section of the plate stack.

The motion of fluids is an important aspect of energy conversion. Fig. (**10**) represents the velocity variation at the cross-section of the stack channel. The direction of velocity is the x-axis. At several critical moments, the

motion of the fluid is periodic and reciprocating, which is also the dynamic mechanism of its heat exchange with the plate stack. Obviously, the motion changes at the center of the stack channel are more sensitive, which is caused by the effect of the boundary layer. However, the most sensitive location for fluid motion is not in the center, but on the side of the viscous layer. This is because the fluid closer to the plate stack has better heat transfer characteristics, but the flow still needs to overcome the influence of the boundary layer.

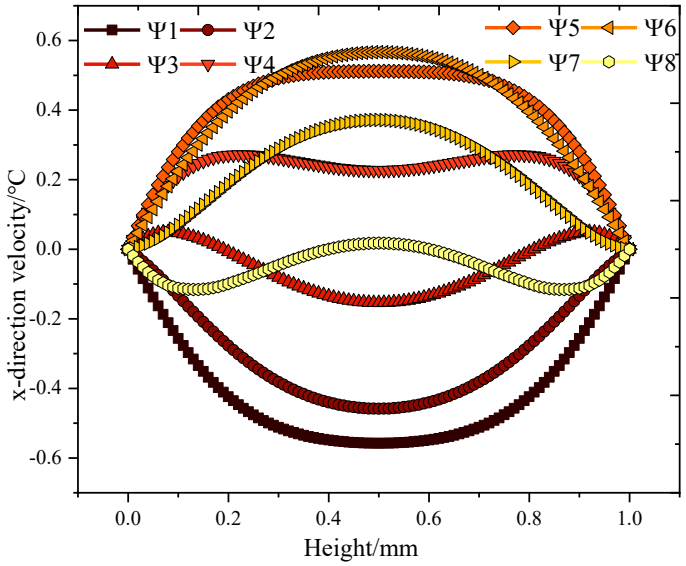

Figure 10: The velocity variation at the cross-section of the stack channel.

Due to the fact that sound waves are standing waves, thermoacoustic engines exhibit periodic velocity distributions in the transverse direction. Fig. (**11**) shows the lateral velocity distribution characteristics of the thermoacoustic device during the acoustic cycle. The vertical axis represents the velocity magnitude in the x direction, and the horizontal axis represents the transverse intercept length of the thermoacoustic engine passing through point A. Obviously, the change in velocity laterally is also periodic. Due to the blockage of the flow caused by the stacks, the velocity at the channel of the stacks varies greatly, which is different from the velocity inside the resonant tube. Due to the fact that the thermoacoustic device is a standing wave thermoacoustic engine with an open end. The flow velocity at the opening reaches its maximum.

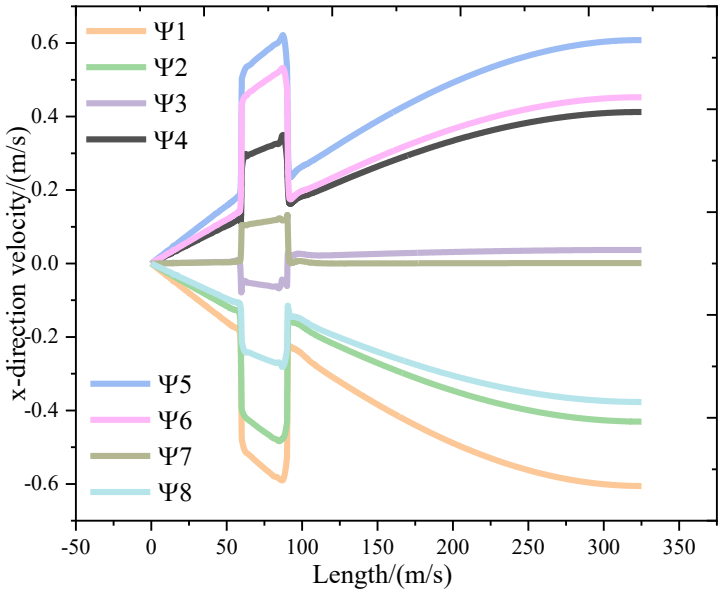

Figure 11: The lateral velocity distribution characteristics of the thermoacoustic device during the acoustic cycle.

Fig. (**12**) shows the temperature of the fluid and the surface temperature of the plate stack. The temperature positions are the surface of the stack and the center of the stack channel. In numerical simulation, the temperature change rate of the plate stack is constant. Due to the heat exchange and energy transfer between fluids and plate stacks, the temperature of fluids is affected by nonlinear dissipation. The dissipation of energy is mainly concentrated at the edge of the plate stack, which is also an area of unstable flow.

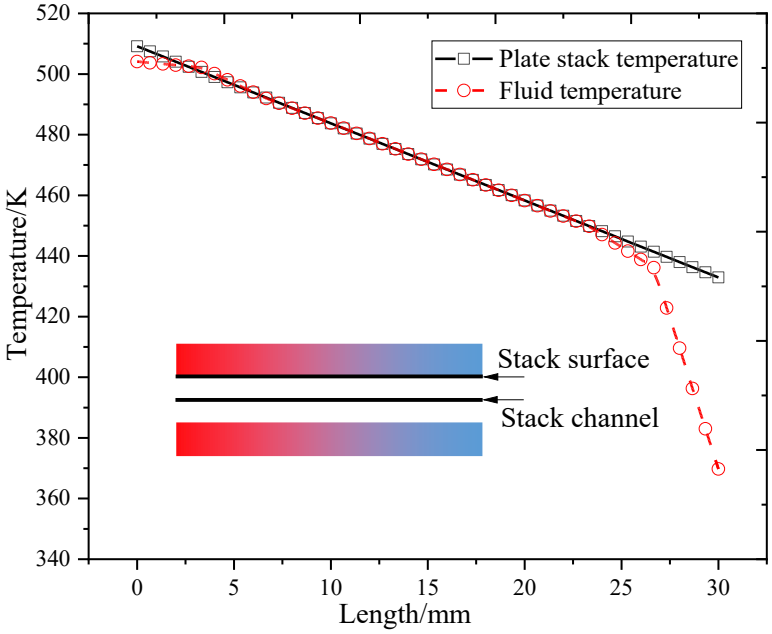

Figure 12: The temperature of the fluid and the surface temperature of the plate stack.

Due to the periodic nature of thermoacoustic effects, it is necessary to introduce time averaged methods to study the variation characteristics of key parameters. The heat flux can be expressed as:

$$q(x,t) = -k\frac{dT}{dy}\bigg|_{x,t} \tag{12}$$

$$\bar{q}_t = \int_{x_c}^{x_h} q(x,t)\,dx \tag{13}$$

$$\bar{q}_x = \frac{w}{2\pi}\int_t^{t+\frac{2\pi}{w}} q(x,t)dt \tag{14}$$

where, $\bar{q}_x$ $\bar{q}_t$ and $q(x,t)$ are the time-average heat flux, the instantaneous total heat flux and the instantaneous heat at the location *x*, respectively; *w* and *t* are angular frequency and time, respectively. The subscripts "h" and "c" respectively indicate the positions of the hot and cold ends of the stack.

Fig. (**13**) shows the time averaged heat flux on the surface of the plate stack. At the hot end of the stack, the fluid absorbs the heat of the stack and expands, causing the fluid to do work on the outside. At the cold end of the stack, the stack absorbs heat from the fluid and contracts, causing external work to be done on the fluid. In addition, due to the unstable heat transfer between the fluid and the plate stack, there are also some heat flux peaks caused by heat transfer between the fluid and the plate stack.

3.3. Multi Physical Field Characteristics of Thermoacoustic Conversion

Thermoacoustic effect is the conversion between thermal energy and acoustic energy, which involves changes in temperature, pressure, and velocity. The thermoacoustic effect involves periodic heat and mass transfer, with the plate stack being the core of thermoacoustic conversion. Compare the temperature, velocity, and pressure

changes at point A at the center of the stack (Fig. **3**). Fig. (**14**) shows the changes in pressure, velocity, and temperature during the thermoacoustic conversion process under stable conditions. For better comparison, the three parameters were dimensionless. The phase difference between pressure and velocity is 90°. The phase difference between velocity and temperature is one phase. The changes in each parameter exhibit a sinusoidal trend. From the perspective of Lagrange's assumption, assuming that the fluid is actually composed of countless small air masses, when a stacked plate with a temperature difference is introduced as the second medium, the motion process of the small air masses between the plate stacks can be approximated as a thermodynamic cycle process [51].

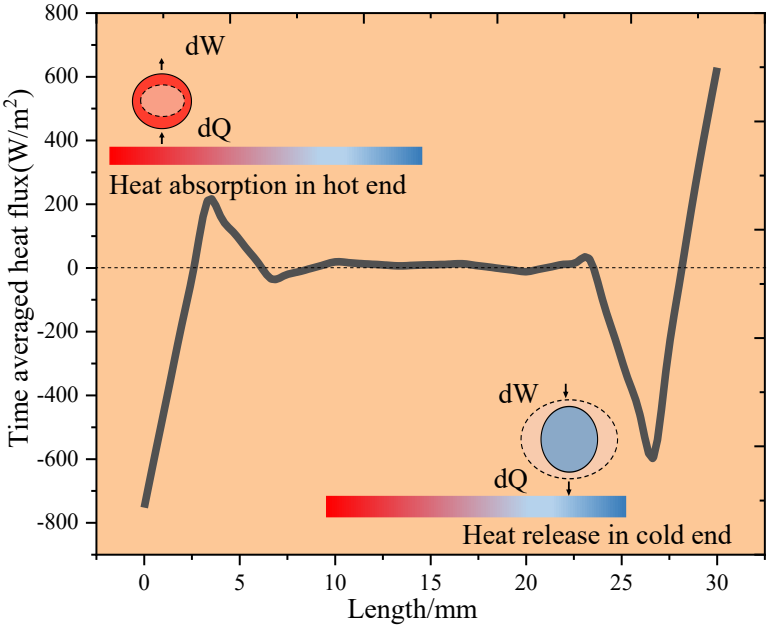

Figure 13: The time averaged heat flux on the surface of the plate stack.

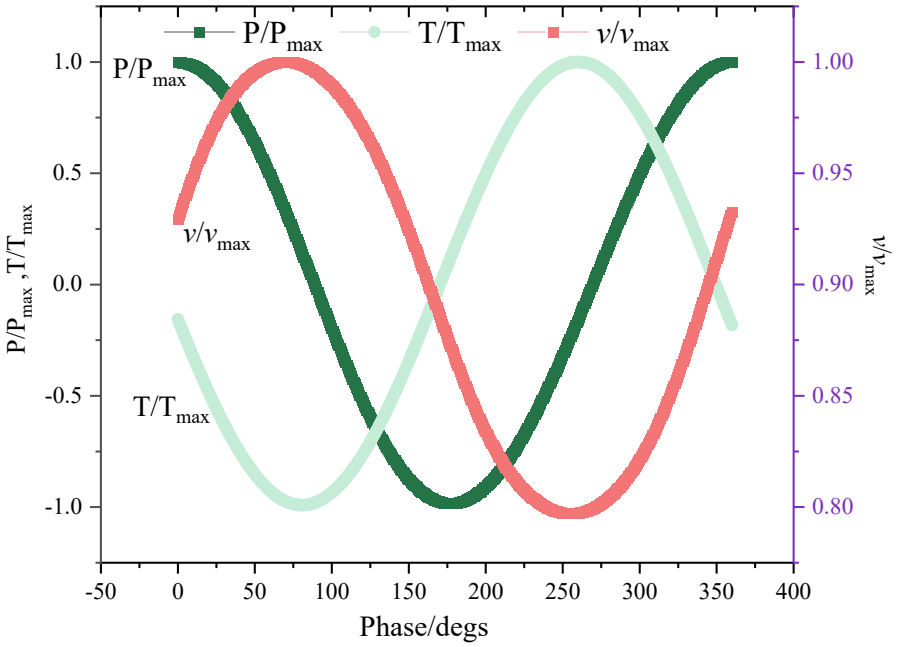

Figure 14: The changes in pressure, velocity, and temperature during the thermoacoustic conversion process under stable conditions.

Due to the complex nonlinear temperature field distribution and non isothermal eddy currents in thermoacoustic machinery, linear thermoacoustic theory exhibits significant limitations in self-excited oscillation and low-frequency high amplitude thermoacoustic conversion. Numerical simulation methods can effectively demonstrate the nonlinear characteristics of thermoacoustic heat engines. Fig. (**15**) shows the temperature and flow field characteristics near the plate stack at different times. In the numerical model, the gas density is represented as $\rho = f(p,T)$. Fig. (**15a**-**d**) correspond to the temperature and flow field distributions at 0.1 s and 0.3 s, respectively. The arrows in the figure indicate the magnitude and direction of the velocity. During the oscillation period of the thermoacoustic engine, due to the high temperature of the heat exchanger at the hot end, the temperature of the surrounding gas increases, and the gas density and pressure change, resulting in thermal convection in the gas chamber and resonance tube. Outside the stacked channel, due to the inertia effect, heat exchange occurs between the high-temperature fluid and the low-temperature fluid further away, forming Rayleigh flow. Due to the nonlinear fluid effects and irreversible thermal processes caused by high-intensity acoustic oscillations, these effects disrupt the ideal thermal acoustic coupling phase.

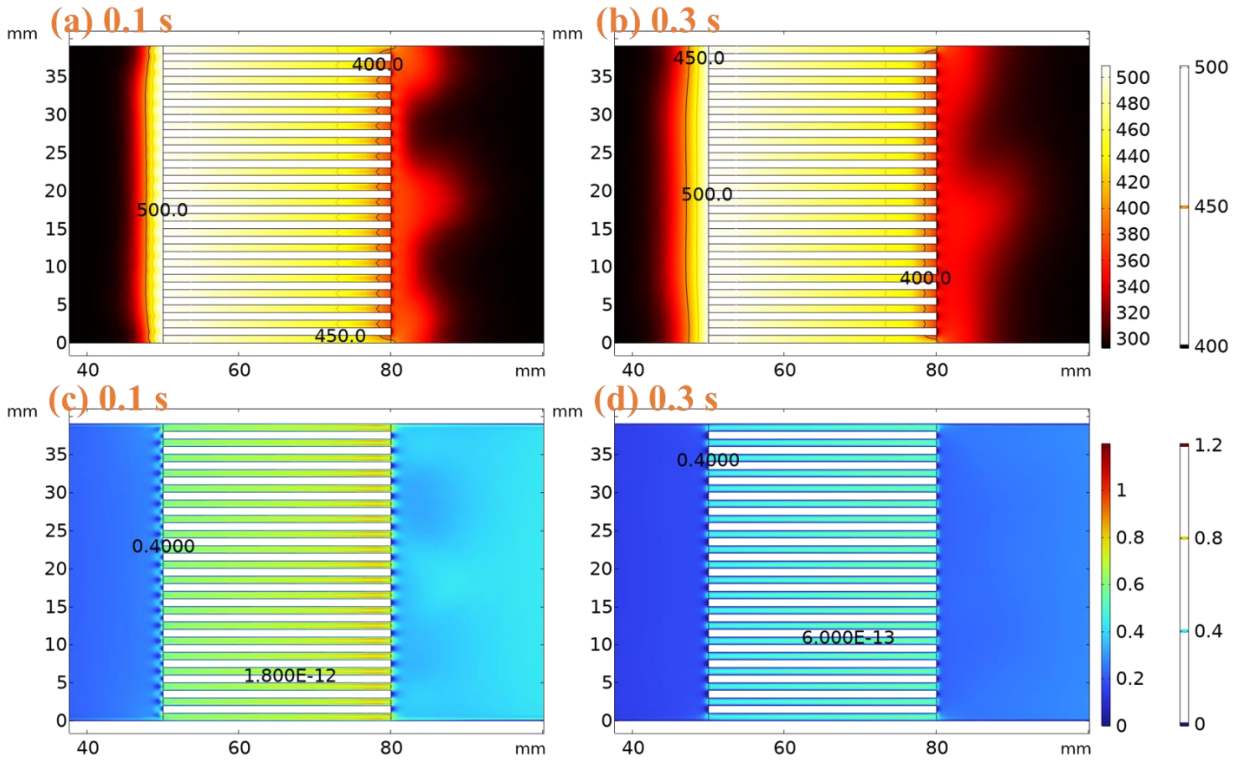

Figure 15: The temperature and flow field characteristics near the plate stack at different times (temperature, K; velocity, m/s).

Fig. (**16**) shows the distribution of velocity fields at the edge of the board stack of the thermoacoustic detection alarm device. It can be seen that due to boundary viscous resistance and the stagnation of fluid flow at the front edge of the plate stack at x=82 mm, a narrow vortex cluster appears in the upper part of the fluid (Ψ3). According to the velocity vector, the velocity decreases near the vortex cluster because the vortex cluster obstructs gas flow, resulting in a decrease in velocity. Vortex clusters consume fluid kinetic energy, affect temperature transfer, and thus reduce energy conversion at the hot end (Ψ7). The high-temperature fluid at the hot end moves towards the cold end, forming a high-temperature jet like flow zone at the channel (Ψ5, Ψ6). Multiple vortices formed at the edge of the stack. In fact, the viscous dissipation caused by fluid motion and vortices leads to the nonlinear energy dissipation of thermoacoustic thermal engines, which is one of the important reasons restricting the energy conversion rate of this type of machinery [52] (Ψ7). In the Ψ7 of Fig. (**16**), the jet flow at the edge of the stacked channel is discovered. Jet flow is a typical nonlinear flow in thermoacoustic devices. Due to the non slip state at the boundary, it is evident that there is a reflux phenomenon in the Stokes layer within the stacked channel and at the sudden change in cross-section after stacking.

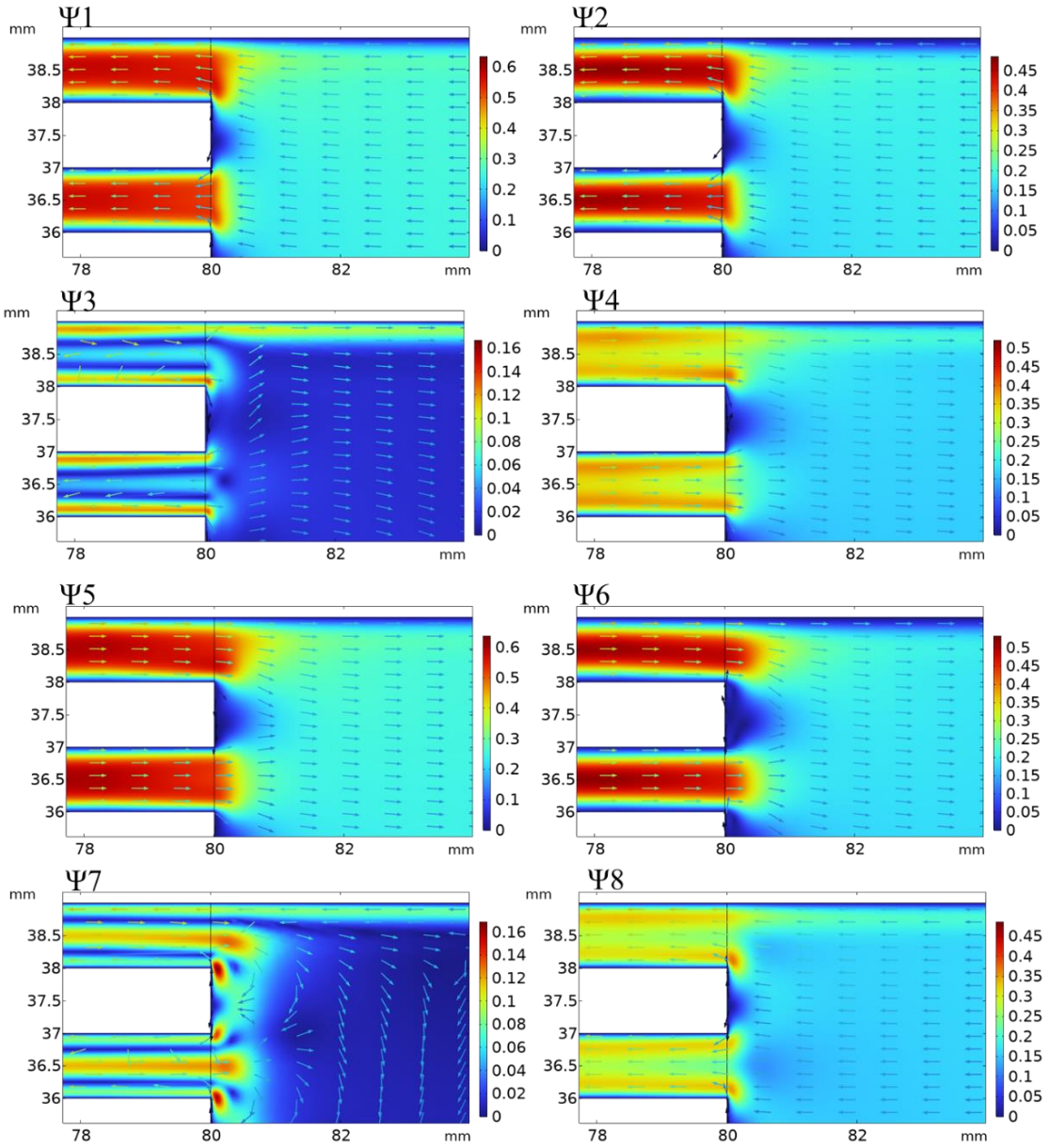

Figure 16: The distribution of velocity fields at the edge of the board stack of the thermoacoustic detection alarm device (velocity, m/s).

Fig. (**17**) shows the distribution of temperature fields at the edge of the board stack of the thermoacoustic detection alarm device. The current numerical model has weak sound pressure and flow intensity, and there is little difference in temperature distribution at the edge of the plate stack at different stages. Due to the high flow velocity, there is no perfect heat transfer between the high-temperature fluid and the plate stack. Some high-temperature fluids flow from the cold end heat exchanger to the outside of the plate stack, which is an important aspect of the heat dissipation of the thermoacoustic heat engine.

4. Conclusions

A fire detection and alarm device based on thermoacoustic effect has been developed for the prevention of building fires. This work introduces the basic theory of thermoacoustics and elaborates on the application of thermoacoustic engines in fire detection. The design requirements of the thermoacoustic engine were summarized, and a fire detection and alarm device based on the thermoacoustic effect was developed.

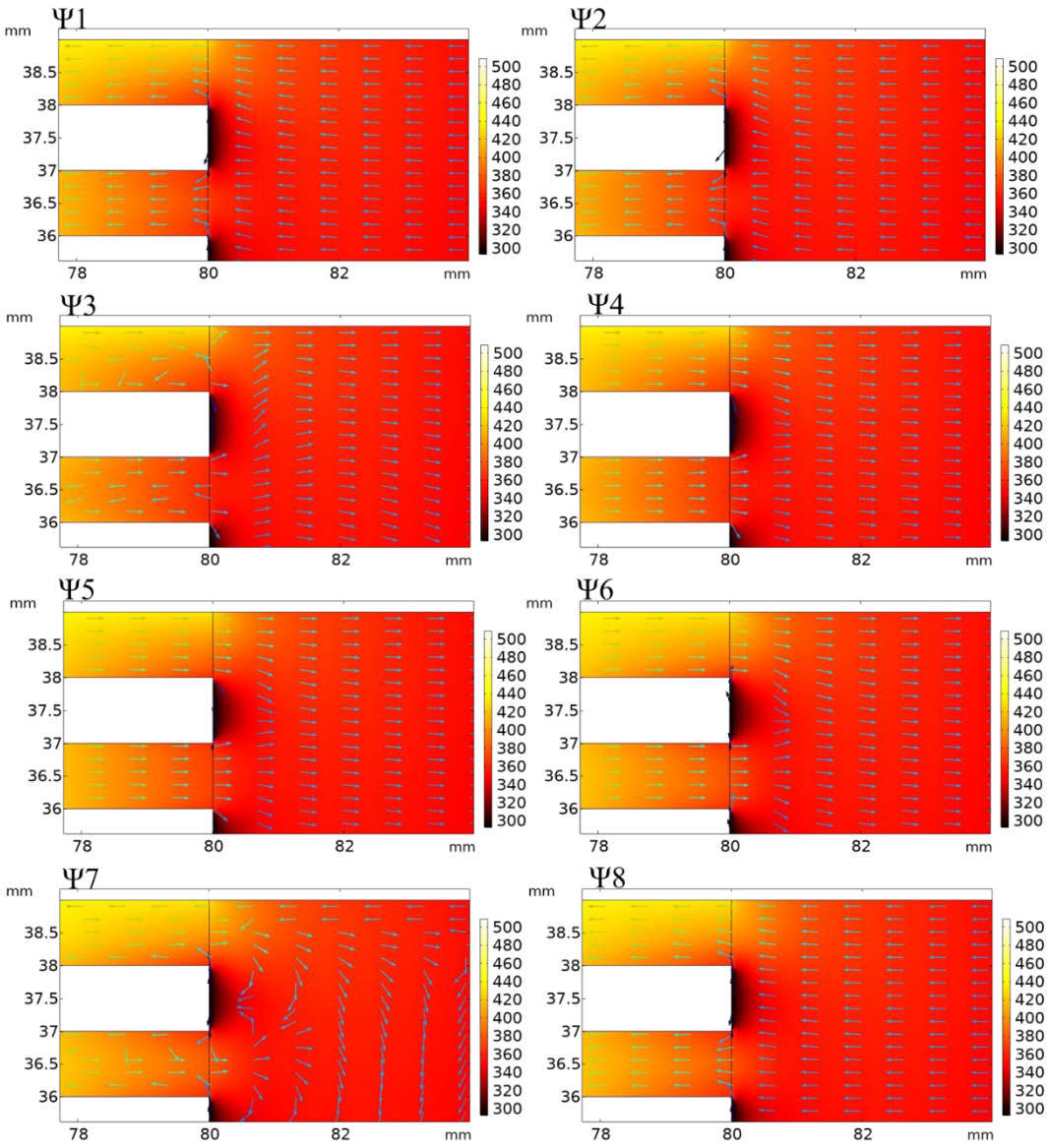

Figure 17: The distribution of temperature fields at the edge of the board stack of the thermoacoustic detection alarm device (temperature, K).

The sound pressure level varies in three stages with the temperature difference at both ends of the heat exchanger, namely energy storage, rapid rise, and saturation stage. At the initial sound level, the sound pressure level can reach 120 dB, and after saturation, it stabilizes at around 125.3 dB, with a frequency of 281.3 Hz, which can meet the alarm requirements. Under the condition of the lowest temperature difference that can produce sound, the sound pressure level can reach 121 dB and stabilize at around 125.3 dB after saturation, with a frequency of 281.3 Hz. By simulating the coupling of multiple physical fields, the coupling state between heat and flow in the thermoacoustic detection alarm device is obtained. Numerical simulation can effectively demonstrate the nonlinear vortices at the edge of the stack and the heat dissipation towards the outside of the stack.

Thermoacoustic engines have great potential in fire alarm applications due to their lack of moving parts, low power consumption, and environmental friendliness. However, future work is needed to overcome the measurement and optimization of device parameters.

Conflict of interest

The authors declare no conflict of interest.

Funding

The authors would like to express their deepest appreciation for the support given by the China Postdoctoral Science Foundation (2023M733276), the Fundamental Research Program of Shanxi Province, China (202303021212202), Heilongjiang Provincial Natural Science Foundation of China (No. LH2021B006), The National Natural Science Foundation of China (No. 22205049) and Shaanxi Provincial Outstanding Youth Science Foundation Program (Grant No. 2025JC-JCQN-024).

Acknowledgments

The authors would like to express their deepest appreciation for all the financial supporters.

References

[1] Barillo DJ, Goode R. Fire fatality study: demographics of fire victims. Burns. 1996, 22: 85-8. https://doi.org/10.1016/0305-4179(95)00095-X

[2] Król A, Szewczyński K, Król M, Koper P, Bielawski J, Węgrzyński W. Full-scale experimental, numerical, and theoretical research on the spatio-temporal evolution of the flow structure in longitudinal and semi-transversal ventilated tunnels. Tunn Undergr Space Technol. 2024; 147: 105721. https://doi.org/10.1016/j.tust.2024.105721

[3] Jiang Y, Li G, Wang J. Photoacoustic compound fire alarm system for detecting particles and carbon monoxide in smoke. Fire Technol. 2016; 52(5): 1255-69. https://doi.org/10.1007/s10694-015-0542-6

[4] Qiu X, Wei Y, Li N, Guo A, Zhang E, Li C, *et al*. Development of an early warning fire detection system based on a laser spectroscopic carbon monoxide sensor using a 32-bit system-on-chip. Infrared Phys Technol. 2019; 96: 44-51. https://doi.org/10.1016/j.infrared.2018.11.013

[5] Swift GW. Thermoacoustic engines. J Acoust Soc Am. 1988; 84: 1145-80. https://doi.org/10.1121/1.396617

[6] Wen J, Zhang L, Kan H, Liu S, Wang K. Advances in the utilization and suppression of thermoacoustic effect: A review. Int J Heat Mass Tranf. 2024; 231: 125758. https://doi.org/10.1016/j.ijheatmasstransfer.2024.125758

[7] Wigdan K, Paul R, Jon M, David H. Asymmetrically heated multi-stage travelling-wave thermoacoustic electricity generator. Energy. 2021; 235: 121312. https://doi.org/10.1016/j.energy.2021.121312

[8] Hiroshi Y, Yasuaki O, Masashi K, Masahito N, Hideki Y. Simulation of thermoacoustic heat pump effects driven by acoustic radiation in a cavity flow. Int J Heat Mass Tranf. 2022; 185: 122424. https://doi.org/10.1016/j.ijheatmasstransfer.2021.122424

[9] Hu Y, Chi J, Wu Z, Zhang L, Yang R, Xu J, *et al*. Study on a high-performance heatdriven thermoacoustic heat pump. Appl Therm Eng. 2024, 253: 123790. https://doi.org/10.1016/j.applthermaleng.2024.123790

[10] Ali U, Al-Mufti O, Janajreh I. Harnessing sound waves for sustainable energy: Advancements and challenges in thermoacoustic technology. Energy Nexus. 2024; 15: 100320. https://doi.org/10.1016/j.nexus.2024.100320

[11] Chi J, Xu J, Zhang L, Wu Z, Hu J, Luo E. Study of a gas-liquid-coupled heat-driven room-temperature thermoacoustic refrigerator with different working gases. Energy Convers Manage. 2021; 246: 114657. https://doi.org/10.1016/j.enconman.2021.114657

[12] Nathan B. Michael L. Steven F. Ramon GZ. High-fidelity numerical simulations of a standing-wave thermoacoustic engine. Appl Energy. 2024; 360: 122817. https://doi.org/10.1016/j.apenergy.2024.122817

[13] Liu L, Cai J, Liu Y. Structural optimization of resonance tubes for a looped thermoacoustic engine with multiple heat sources. Case Stud Therm Eng. 2023; 49: 103344. https://doi.org/10.1016/j.csite.2023.103344

[14] Chen G, Li Z, Li X, Xu J, Sun W, Tang L, *et al*. Optimal cross-sectional area ratio between porous material and resonance tube for the onset of self-excited oscillations in standing-wave thermoacoustic engines. Therm Sci Eng Prog. 2023; 41: 101856. https://doi.org/10.1016/j.tsep.2023.101856

[15] Jesse C, Revant A, Mohamed M, Mostafa N. Traveling wave thermoacoustic refrigeration with variable phase-coordinated boundary conditions. J Acoust Soc Am. 2024; 154(6): 3943-54. https://doi.org/10.1121/10.0023954

[16] Backhaus S, Swift GW. A thermoacoustic Stirling heat engine. Nature. 1999; 399: 335-8. https://doi.org/10.1038/20624

[17] Rayleigh L. The theory of sound. UK: Dover Publication, 1896.

[18] Zhu Q, Yu J, Zhu H. The influence of thermoacoustic effect and microstructure parameters on acoustic performance of porous ceramic fiber material. Appl Acoust. 2025; 240(5): 110915. https://doi.org/10.1016/j.apacoust.2025.110915

[19] Rott N. Damped and thermally driven acoustic oscillations in wide and narrow tubes. J Appl Math Phys. 1969; 20(2): 230-40. https://doi.org/10.1007/BF01595562

[20] Roberto B, Armando DM, Antonio F, Nicola M. Design and performance of a ThermoAcoustic Electric Generator powered by waste-heat based on linear and nonlinear modelling. Appl Therm Eng. 2025; 276: 126938. https://doi.org/10.1016/j.applthermaleng.2025.126938

[21] Prashantha BG, Seetharamu S, Narasimham GSV, Manjunatha K. Effect of gas spacing and resonance frequency on theoretical performance of thermoacoustic refrigerators. Int J Air-Cond Refrig. 2023; 31(1): 1-14. https://doi.org/10.1007/s44189-023-00027-7

[22] Yao C, Liu J, Yan J. Numerical investigation of nonlinear effects in a standing wave thermoacoustic engine using the discontinuous Galerkin method. Int J Heat Mass Tran. 2023; 216: 124526. https://doi.org/10.1016/j.ijheatmasstransfer.2023.124526

[23] Zhang D, Guan J, He Z, Shen C, Li H, Tang S, *et al*. Numerical analysis of thermoacoustic heat pump driving by prime mover. Heat Transf Res. 2025; 56(3): 15-29. https://doi.org/10.1615/HeatTransRes.2024053033

[24] Guo L, Zhao D, Yu D, Xu J, Su Y, Sun D, *et al*. Energy conversion performance in looped and stirling traveling-wave and standing-wave thermoacoustic engines. Appl Therm Eng. 2024; 258: 124622. https://doi.org/10.1016/j.applthermaleng.2024.124622

[25] Diana BC, Yann F, Catherine W. Gravity effects in a compact thermoacoustic cavity. J Acoust Soc Am. 2025; 157(2): 833-44. https://doi.org/10.1121/10.0035581

[26] Nathan B, Michael L, Steven F, Ramon GZ. High-fidelity numerical simulations of a standing-wave thermoacoustic engine. Appl Energy. 2024; 360: 122817. https://doi.org/10.1016/j.apenergy.2024.122817

[27] Symko OG, Abdel-Rahman E, Kwon YS, Emmi M, Behunin R. Design and development of high-frequency thermoacoustic engines for thermal management in microelectronics. Microelectron J. 2004; 35(2): 185-91. https://doi.org/10.1016/j.mejo.2003.09.017

[28] Shen C, He Y, Li Y, Ke H, Zhang D, Liu Y. Performance of solar powered thermoacoustic engine at different tilted angles. Appl Therm Eng. 2009; 19(13): 2745-56. https://doi.org/10.1016/j.applthermaleng.2009.01.008

[29] Emmanuel CN, Azrai A. Experimental study on the performance of the thermoacoustic refrigerating system. Appl Therm Eng. 2009; 29(13): 2672-9. https://doi.org/10.1016/j.applthermaleng.2008.12.036

[30] Buda-Ortins KE. Prototype design for thermoacoustic flashover detector (Thesis). The University of Maryland; 2012. Available from: http://hdl.handle.net/1903/13069

[31] Hamburger KA. Optimization and implementation of a thermoacoustic flashover detector (Thesis). The University of Maryland; 2013. Available from: http://hdl.handle.net/1903/14795

[32] Jeffrey ZT. Response of a thermoacoustic flashover detector to thermal radiation (Thesis). The University of Maryland; 2014. https://doi.org/10.13016/M2DG7V

[33] Pan N, Wang S, Shen C. A fundamental study on characteristic of thermoacoustic engine with different tilt angles. Int J Heat Mass Tranf. 2014; 74: 228-37. https://doi.org/10.1016/j.ijheatmasstransfer.2014.03.019

[34] Kenichiro T, Yuki U. Critical temperature of traveling- and standing-wave thermoacoustic engines using a wet regenerator. Appl Energy. 2017; 196: 62-7. https://doi.org/10.1016/j.apenergy.2017.04.004

[35] Raspet R, Slaton WV, Hickey CJ, Hiller RA. Theory of inert gas-condensing vapor thermoacoustics: Transport equations. J Acoust Soc Am. 2002; 112(4): 1414-22. https://doi.org/10.1121/1.1508113

[36] Rogozinski K, Nowak I, Nowak G. Modeling the operation of a thermoacoustic engine. Energy. 2017; 138: 249-56. https://doi.org/10.1016/j.energy.2017.07.058

[37] Jaworski AJ, Mao X, Mao X, Yu.Z. Entrance effects in the channels of the parallel plate stack in oscillatory flow conditions. Exp Therm Fluid Sci. 2009; 33: 495-502. https://doi.org/10.1016/j.expthermflusci.2008.11.003

[38] Kuzuu K, Hasegawa S. Effect of non-linear flow behavior on heat transfer in a thermoacoustic engine core. Int J Heat Mass Tranf. 2017; 108: 1591-601. https://doi.org/10.1016/j.ijheatmasstransfer.2016.12.064

[39] Jung S, Matveev KI. Study of a small-scale standing-wave thermoacoustic engine. Proc Inst Mech Eng C J Mech Eng Sci. 2010; 224(1): 133-41. https://doi.org/10.1243/09544062JMES1594

[40] Hao XH, Ju YL, Behera U, Kasthurirengan S. Influence of working fluid on the performance of a standing-wave thermoacoustic prime mover. Cryogenics. 2011; 51(9): 559-61. https://doi.org/10.1016/j.cryogenics.2011.07.004

[41] Tang K, Huang ZJ, Jin T, Chen GB. Influence of acoustic pressure amplifier dimensions on the performance of a standing-wave thermoacoustic system. Appl Therm Eng. 2009; 29(5-6): 950-6. https://doi.org/10.1016/j.applthermaleng.2008.05.001

[42] Mumith JA, Mkatsori C, Karayiannis TG. Design of a thermoacoustic heat engine for low temperature waste heat recovery in food manufacturing. Appl Therm Eng. 2014; 65(1-2): 588-96. https://doi.org/10.1016/j.applthermaleng.2014.01.042

[43] Zhang D, He Y, Yang W, Gu X, Wang Y, Tao W. Experimental visualization and heat transfer analysis of the oscillatory flow in thermoacoustic stacks. Exp Therm Fluid Sci. 2013; 46: 221-31. https://doi.org/10.1016/j.expthermflusci.2012.12.014

[44] Chen G, Kai W, Liu L, Gao L, Li Z, Tang L. Experimental evaluation of an integrated thermoacoustic stack. Therm Sci Eng Prog. 2025; 64: 103810. https://doi.org/10.1016/j.tsep.2025.103810

[45] Giulio ED, Meglio AD, Massarotti N, Romano RA, Dragonetti R. Oriented fibers stacks for thermoacoustic devices. Appl Energy. 2024; 373: 123959. https://doi.org/10.1016/j.apenergy.2024.123959

[46] Zhang Y, Shi X, Li Y, Zhang Y, Liu Y. Characteristics of thermoacoustic conversion and coupling effect at different temperature gradients. Energy. 2020; 197(15): 117228. https://doi.org/10.1016/j.energy.2020.117228

[47] Blanc N, Laufer M, Frankel S, Ramon GZ. High-fidelity numerical simulations of a standing-wave thermoacoustic engine. Appl Energy. 2024; 360(15): 122817. https://doi.org/10.1016/j.apenergy.2024.122817

[48] Hireche O, Weisman C, Baltean-Carlès D. Numerical model of a thermoacoustic engine. C R Mec. 2010; 338: 18-23. https://doi.org/10.1016/j.crme.2009.12.006

[49] Yu G, Dai W, Luo E. CFD simulation of a 300 Hz thermoacoustic standing wave engine. Cryogenics. 2010; 50: 615-22. https://doi.org/10.1016/j.cryogenics.2010.02.011

[50] Wang K, Tao S, Li Z, Li X, Tang L, Chen G. Investigation on the hysteresis behavior of a quarter-wavelength standing-wave thermoacoustic engine. Proc Inst Mech Eng C J Mech Eng Sci. 2025; 290(15): 110084. https://doi.org/10.1016/j.ijmecsci.2025.110084

[51] Niu Y, Zhang H, Jiang H, Hu L, Liu Y. Numerical studies on mode transition and performance of the thermoacoustic engine coupled with acoustic pressure amplifier tube and load. Energy. 2024; 307(30): 132746. https://doi.org/10.1016/j.energy.2024.132746

[52] Vorotnikov GV, Zinovyev EA, Nekrasova SO. Thermodynamic cycle of the traveling wave thermoacoustic engine. Case Stud Therm Eng. 2022; 36: 102216. https://doi.org/10.1016/j.csite.2022.102216